Molecular dynamics simulation of graphene on Cu (1 0 0) and (1 1 1) surfaces

Klaver, TPC; Zhu, S; Sluiter, MHF; Janssen, GCAM

DOI
10.1016/j.carbon.2014.11.005

Publication date
2015

Document Version
Accepted author manuscript

Published in
Carbon

Citation (APA)
Klaver, TPC., Zhu, S., Sluiter, MHF., & Janssen, GCAM. (2015). Molecular dynamics simulation of graphene on Cu (1 0 0) and (1 1 1) surfaces. *Carbon*, *82*, 538-547. https://doi.org/10.1016/j.carbon.2014.11.005

Important note
To cite this publication, please use the final published version (if applicable).
Please check the document version above.

Link to formal publication "Carbon" (Elsevier): https://doi.org/10.1016/j.carbon.2014.11.005

published in Carbon 82 (2015) p538–547

Molecular dynamics simulation of graphene on Cu (100) and (111) surfaces

T. P. C. Klaver[1]*, Shou-En Zhu[2], M. H. F. Sluiter[1], G. C. A. M. Janssen[2]

[1] Department of Materials Science and Engineering, Delft University of Technology, Mekelweg 2, 2628 CD Delft, Netherlands

[2] Department of Precision and Microsystems Engineering, Delft University of Technology, Mekelweg 2, 2628 CD Delft, Netherlands

Abstract

We present results of molecular dynamics simulations of graphene on Cu surfaces. Interactions were modelled with the Charge Optimized Many Body potential, which gives a reasonable though not flawless description of the graphene-Cu system. The interaction between Cu and complete graphene sheets is characterized by an 'averaged out' interaction at a large bonding distance. Many bonding characteristics are indifferent to the details of how the Cu surface atoms are arranged, including the surface orientation and even if the surface is solid or molten. Graphene edges have a strong interaction with the Cu substrates. Systems were modelled at various temperatures, ranging from 0 K to the Cu melting temperature. At high temperature we find that the presence of graphene slightly stabilizes the Cu surface and retards surface melting. After cooling down to room temperature, the Cu substrate is 1.7% smaller than the graphene due to difference thermal expansion coefficients. This leads to the formation of wrinkles in graphene. Single wrinkles experience only small migration barriers and are quite mobile. When multiple wrinkles intersect, they form immobile knots that hinder further movement of the connected wrinkles. The elastic energy of the wrinkles and knots due to bending of the graphene is determined.

1 Introduction

The extraordinary properties of graphene have lead to a very large amount of research on the topic after the publication of the landmark work [1] by Novoselov *et al*. Many different experimental methods, theoretical models and simulation techniques have been employed to study the properties of graphene. Apart from studying the properties of isolated graphene sheets, their production has also been the subject of extensive research. While early experiments used mechanical exfoliation with Scotch tape to produce single or few layer thick graphene samples, this process is not well suited for industrial production. Graphene growth through chemical vapour deposition (CVD) on solid surfaces or growth from C supersaturated substrates or through liquid phase exfoliation of graphite are much more promising methods in that respect. Despite the extensive research already done on CVD of graphene on Cu substrates, questions remain. Some observations have lead to conflicting explanations, while others are not explained very well at all. Some examples of such not yet (fully) resolved issues are the role of hydrogen in the gas mixture [2, 3, 4], the interaction of graphene with Cu under different orientations [5], the influence of temperature on growth [6] and the diffusion of C atoms and clusters during graphene growth. [7]. Atomistic simulations offer detailed insight into processes occurring at atomic length and time scales. We have carried out classical molecular dynamics (MD) simulations of graphene on bare Cu (100) and (111) surfaces, to complement CVD-on-Cu experiments done in our group [8]. The empirical potentials required to model graphene on Cu must meet some rather tough requirements. In section 2 of this paper we will explain our choice of the charge optimised many-body potential (COMB) [9, 10] and provide details of how simulations were carried out. In section 3.1 we first present and discuss results of how the COMB potential describes various properties of the graphene/Cu system. We then present simulations results of graphene on Cu at high temperature that is close to the melting temperature. Finally in section 3.3 we look at the graphene/Cu system once it has cooled down, and a size mismatch between Cu and graphene must be accommodated. The excess graphene resulting from the size mismatch leads to the formation of wrinkles. We compare

the wrinkles observed in our simulations to similar types of wrinkles seen in experiments. A summary is given in section 4.

2 Computational details

Atomistic modelling of graphene-on-Cu requires an interaction potential capable of describing different types of interactions. It involves metallic interaction for Cu, covalent interaction for graphene, and weak van der Waals interaction between complete graphene layers and Cu. Of these interactions, the Cu-Cu interaction is commonly described by an embedded atom method (EAM) potential [11, 12], the C-C interaction is most often described by the widely used REBO2 [13] or AIREBO [14] potentials and the van der Waals interaction is often modelled by a Lennard-Jones (LJ) potential. The combination of using REBO2/AIREBO for modelling graphene and LJ bonding of the graphene to a solid surface is commonly used [see e.g. 15-20] and would also be sufficient for our simulations of complete graphene monolayers on Cu surfaces. However, this approach does impose restrictions. While complete graphene sheets only interact with the Cu surface through weak van der Waals interaction, C atoms on the edges of graphene islands have unsaturated bonds that can have a strong interaction with the Cu surface. Hence, the C-Cu interaction should ideally be capable of reproducing both of these different interaction regimes, so that graphene islands can be simulated. If graphene islands are grown through chemical vapour deposition with a methane feedstock, as is done in our group, simulation of such growth would require that C-H and Cu-H interactions are both reproduced by the potential as well, in both the van der Waals and chemical interaction regimes. Additionally, experiments that are not carried out in ultra-high vacuum with purified gasses will include small amounts of oxygen that rapidly interacts with the Cu surface. So ideally, the interaction potential should describe the elements C, Cu, H, and O and all cross interactions between these elements, in different bonding regimes for some element combinations. This is a tall order for any interaction formalism.

Two somewhat recently developed interaction schemes that aim to model a variety of interaction types for a range of elements are the reactive force field (ReaxFF) and COMB formalisms [21]. Both schemes include bond order and variable charge terms, giving them considerable versatility and thus making them promising candidates for modelling the required interactions. However, Wei *et al* [22] benchmarked various potentials for graphene against density-functional theory (DFT) data and found that the ReaxFF potential performed poorly. By contrast, the REBO2 potential performed quite well and the third generation of the COMB potential (COMB3) [9, 10] uses the REBO2 C-C interaction at shorter distances. Also, a parameterisation of the COMB3 formalism has already been successfully used to study hydrocarbons on Cu surfaces [9] as well as surface oxidation of Cu [23]. The parameterisations for C, Cu, H, and O within the COMB3 formalism should therefore allow the simulation of complete graphene sheets on Cu in this work, as well as extending the scope of the simulations to include H and O in future work. For these reasons, we used the COMB3 formalism, as implemented in the widely used MD code LAMMPS [24] in all our MD simulations.

Simulations of Cu surfaces covered by graphene had periodic in-plane dimensions ranging from 46.927 by 54.147 $Å^2$ to 504.56 by 504.56 $Å^2$. Simulation temperatures ranged from 0 K to our maximum experimental temperature of 1323 K (1050 °C). If the average thermal expansion coefficient (TEC) of Cu is estimated to be $1.7*10^{-5}$ in the 300-1323 K range (extrapolated from experimental data for 77 to 973 K [25]), heating Cu from 300 to 1323 K will cause 1.7% expansion. Therefore, three different, fixed Cu lattice parameters were used for simulations at different temperatures. At 0 K, the equilibrium parameter of 0 K was used, from 300 to 500 K the equilibrium lattice parameter at 300 K was used and at temperatures between 1140 K and 1323 K, the equilibrium lattice parameter at 1323 K was used. In contrast to Cu, graphene has a small TEC [26, 27]. At low temperature its in-plane lattice spacing can even slightly contract with rising temperature, despite increasing C-C bond lengths [28]. Therefore its thermal expansion was neglected and the 0 K equilibrium lattice parameter was used at all temperatures. In choosing surface areas, the number of Cu and graphene unit cells was chosen such that graphene could fit on

the Cu with minimal misfit, if the simulation meant to portray stress-free graphene on Cu. The atoms in the bottom layer of the Cu slabs were held fixed to hold the slab and graphene layer on top of it in position. The Cu slabs consisted of 16 Cu monolayers or more. The numbers of Cu and C atoms varied from 6240 and 968 in the smallest system to 627200 and 99840 in the largest. A Nosé-Hoover thermostat was employed to simulate a canonical ensemble (NVT) in MD simulations. The fixed atoms in the Cu bottom layer were excluded from temperature control and reporting. The time step in MD simulations was 0.5 fs, which was small enough for results not to change noticeably when the time step was doubled in a few test simulations. The maximum simulation time was 2 ns. Analysis of surface melting in high temperature simulations was done simply through visual inspection with Ovito [29].

3

3.1 COMB3 description of the graphene/Cu system

Various properties of graphite and Cu were included in the fitting data for the COMB3 potential. The graphene lattice parameter of 1.42 Å is correctly reproduced by the potential. The experimental cohesion energy per C atom in graphite is 7.37 eV and the COMB3 potential predicts a slightly lower cohesion energy of 7.35 eV/C in an isolated graphene sheet. The 3.58 eV/atom cohesion energy and 0 K lattice parameter of 3.61 Å predicted for Cu agree well with the experimental values of 3.54 eV/atom and 3.62 Å [23] to which the potential was fitted. At 300 K and 1323 K, the Cu lattice parameter was 3.63 and 3.70 Å respectively, giving a linear TEC of $1.9*10^{-5}$ in that temperature range, in reasonable agreement with the average extrapolated experimental value of $1.7*10^{-5}$ [25]. The Cu melting temperature was determined through the coexistence method, i.e. running a constant energy simulation of an initially half crystalline, half molten system, where the melting temperature is reached when the molten/solid interface has stopped moving. The Cu bulk melting temperature within the COMB3 model lies between 1140 and 1145 K. This is over 200 K

below the experimental melting temperature of 1358 K. This deviation is more than three times larger than for the computationally much cheaper EAM Cu potential distributed with LAMMPS, which resulted in a Cu melting temperature between 1290 and 1300 K. The calculated Cu (100) and (111) surface energies of 1.52 and 1.27 J/m^2 are somewhat lower than the orientation-averaged experimental value of 1.78 J/m^2 [30]. Our calculated graphene armchair edge energy was slightly higher than the zigzag edge energy (1.27 vs 1.13 eV/ Å), while DFT calculations [31] showed the zigzag edge energy to be higher (1.21 vs. 1.37 eV/ Å).

Beyond pure elements data, we have relaxed nearly stress-free graphene on Cu (100) and (111) surfaces at 0 K. We find that the interaction between graphene and Cu is one that has a fairly large equilibrium distance and that there is no strong interaction between pairs of individual C and Cu atoms. Instead, the interaction is more 'smeared out and generic' over larger numbers of atoms, where every C atom interacts with a number of Cu atoms that are at an approximately similar distance and *vice versa*. The resulting bonding between graphene and Cu surfaces is not very strong and mostly one-dimensional, perpendicular to the Cu surfaces. This picture agrees well with the observation that graphene binds to Cu only weakly [5, 32-36] through physisorption and that graphene (once formed, nucleation and growth may be influenced) is indifferent to the fine details of atomic arrangement of the Cu surface [37].

Even when allowed to fully relax, graphene sheets remained quite flat, not just on close-packed (111) surfaces but also on the more open (100) surfaces where C atoms do not sink significantly into openings between Cu atoms. Because of the generic nature of the interaction, results for both surface orientations are quite similar. The indifference of the graphene layer to which Cu orientation it binds, suggests that different in-plane orientations of the graphene with respect to one particular Cu surface would also not make much difference. This may seem to run counter to the observation that graphene can grow on Cu in preferred orientations [38]. However, it has been suggested [5, 39, 40] that the preferred orientations are determined (in the very early stages of graphene island growth) by the alignment between island edge atoms with unsaturated bonds and rows of Cu surface atoms. Thus, preferred orientations of graphene on Cu surfaces

need not necessarily contradict the finding that large graphene islands would be rather energetically indifferent to their in-plane orientation.
Table 1 list various calculated properties of graphene on Cu (111) and (100) surfaces.

Table 1: Cu-graphene binding distance d, binding energy per C atom E_b, charge accumulation per C atom q_C, maximum height variation for C atoms Δh_C and maximum height variation for Cu surface atoms Δh_{Cu} for graphene on Cu (111) and (100) surfaces, along with electronic structure values from literature for Cu (111).

property	on Cu(111)	electronic structure data on Cu (111)	on Cu(100)
$d_{Cu\text{-}graphene}$ (Å)	3.26	3.58 [a] 3.25 [b] 3.26 [c]	3.22
E_b/C atom (eV)	0.084	0.033 [c] 0.062 [b] 0.038 [a]	0.086
q_C (e^-)	0.04	0.008 [c] 0.004 [a]	0.04
Δh_C (Å)	< 0.01		< 0.02
Δh_{Cu} (Å)	< 0.01		< 0.01

[a] [35]

[b] [41]

[c] [36]

The binding distance is in either reasonable or excellent agreement with electronic structure results. The binding energy is always higher but still of the same order of magnitude compared to electronic structure data. The charge transfer to the C atoms is an order of magnitude greater than that predicted by electronic structure calculations. We also found that putting a net 0.1 electron charge per C atom in isolated graphene increases the C cohesion energy (i.e.

lowers total energy) by 0.3 eV/C atom, which appears unlikely. While systems with net charge are not relevant to our work and probably lie outside what the COMB3 model was constructed for, it does demonstrate a broader tendency of graphene atoms to 'over-zealously' accumulate electronic charge in the COMB3 model. In compensation of the charge on the C atoms, the first few Cu surface layers show an alternating charge depletion/accumulation pattern that rapidly decreases in magnitude deeper into the Cu. The C/Cu areal density ratio is higher for the (100) orientation than for the (111) orientation (2.48 vs. 2.16) and this is reflected in the charge depletion of the Cu surface layers. On the (100) orientation, the charge depletion on Cu atoms in the surface layer is 0.09 electron while on the (111) orientation it is 0.06 electron per Cu atom. The height variation for graphene on Cu is smaller but comparable to the variation of 0.04 Å found for graphene in one particular orientation on Ir, to which graphene also binds weakly [42].

Fig. 1 shows the interaction energy of a graphene sheet with Cu (100) and (111) surfaces as a function of distance.

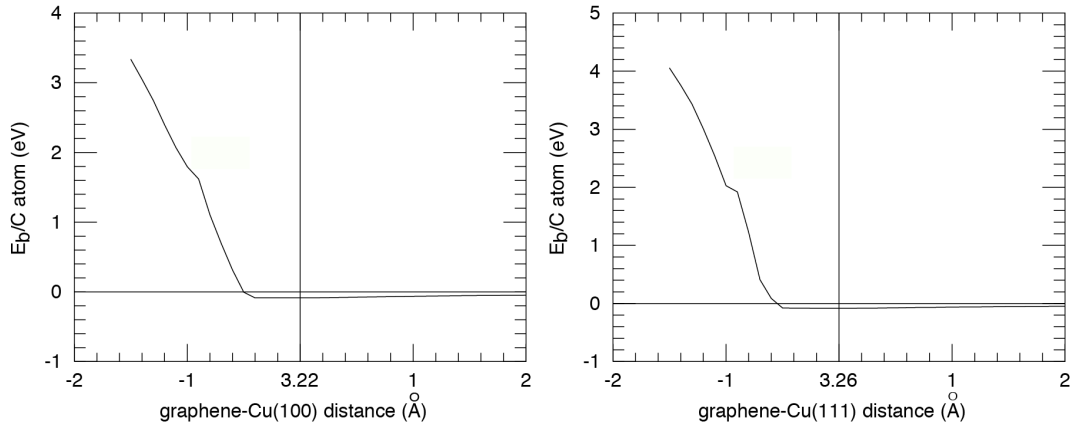

Fig. 1. Interaction energy between graphene and Cu surface as a function of graphene-Cu distance. (a) on Cu (100). (b) on Cu (111).

Fig. 1 shows some features of the C-Cu bonding that seem incorrect. We know of no physical explanation for the shoulder present at ~1 Å compression and suspect that it is an artefact of the COMB3 potential. From ~0.5 Å closer to 2 Å further from the surface than the equilibrium distance, the slope of the energy is almost flat. As a result, the distance between the graphene and Cu surface may

vary considerably with very low energetic cost. The cohesion energy curve calculated with the Random Phase Approximation shows no shoulder and has a much smoother LJ like shape [41]. Also, around 1.5 Å compression the energy curves do not increase more steeply with decreasing distance, as would be expected. For the (111) surface it even levels off slightly. Although the potential certainly has some shortcomings upon closer inspection, the COMB3 model produces graphene that binds to the Cu surface at a very reasonable distance and with a cohesion energy that is of the right order of magnitude. This makes the COMB3 model broadly suitable for our purposes.

3.2 High temperature simulations

Cu (100) and (111) surfaces were annealed up to 2 ns at various temperatures to see at which temperature the substrate would start melting within the short simulation time. For the more open (100) surface the temperature hardly needed to be above the bulk melting temperature. At 1145 K, the substrate had already melted to just above the locked bottom layer in 1.2 ns. By contrast, the close packed (111) surface did not show melting yet after 2 ns if the substrate was held at 1180 K. If held at 1190 K, there was a period where little seemed to happen until there was a melt nucleation event and then the whole substrate very quickly melted almost down to the locked bottom layer. While the observation that the (111) surface forms a greater barrier to melting than the (100) surface makes sense, the big difference in the required overheating is very much an artefact of the requirement that melting starts within the short, 2 ns simulation time. At longer time scales, the melting temperature for the (111) surface would draw much closer to that of the (100) surface.
The binding of graphene to Cu was hardly any less for molten surfaces than for solid surfaces (0.080 eV/C atom on molten Cu compared to 0.086 eV/C on Cu (100) and 0.084 eV/C on Cu (111)), again confirming the indifference of complete, large graphene sheets (nucleation and growth may be different) to the fine details of the underlying Cu surface.

Cu surfaces that were only half covered with graphene were annealed above the melting temperature. The presence of the graphene provides a modest amount of extra cohesion to the surface. The extra cohesion counteracts the melting of Cu. Therefore, in some of our simulations the bare part of the Cu surface had already molten almost down to the locked bottom layer while under the graphene the crystalline planes still reached almost to the surface. This was observed for graphene partially covering both (100) and (111) surfaces, see fig. 2.

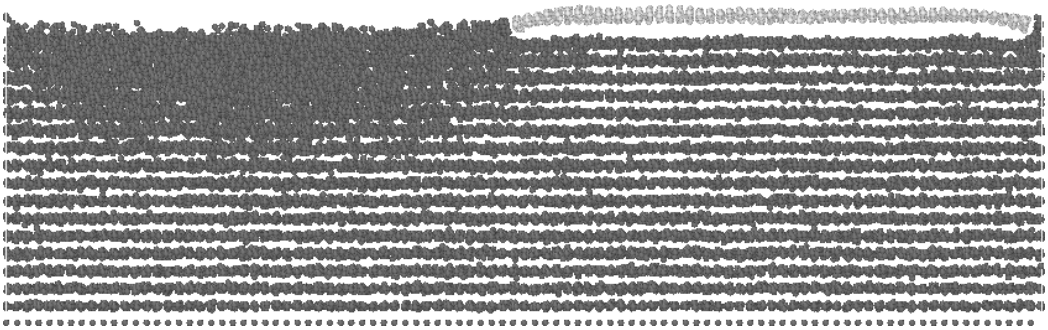

(a)

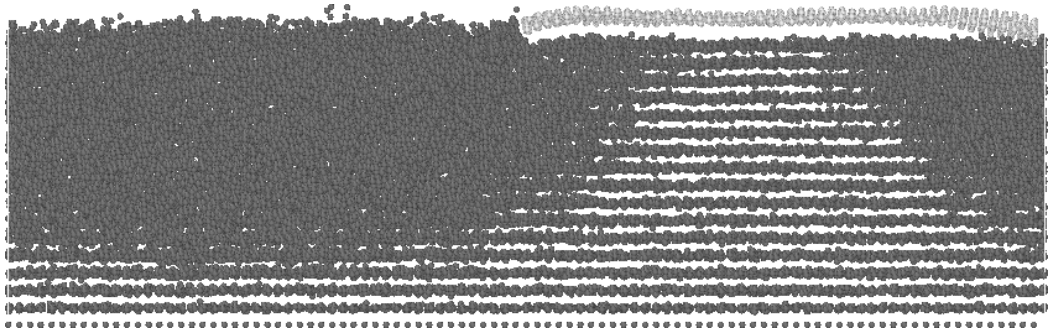

(b)

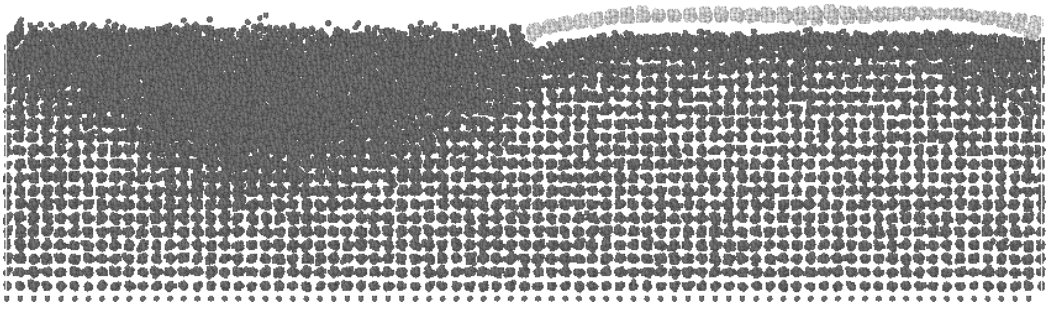

(c)

(d) 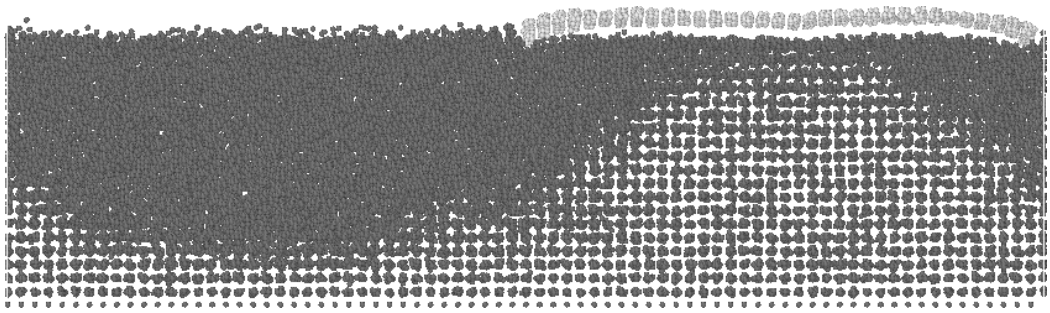

Fig. 2. Melting of Cu (111) and (100) surfaces, half-covered with graphene. a, b: stages of Cu (111) melting. c, d: stages of Cu (100) melting.

Given that the simulation temperatures for both the systems in fig. 2 are above the bulk melting temperature (a few K for Cu (100), tens of K for Cu (111)), both Cu substrates eventually melt down to the locked bottom layer, also under the graphene. However, we can well imagine that in experiments a narrow temperature window exists where the presence of graphene permanently tips the Cu surface from molten to solid. Graphene can be grown on molten Cu [6]. However, we think that in cases where the temperature in such experiments was barely above the melting temperature, a reassessment might be in order. There might be a narrow temperature window where graphene might grow on molten Cu, but that once formed, the graphene stabilises the Cu just enough to turn the surface solid.

It is noteworthy that the edges of the graphene layers in fig. 2 are bending towards the Cu. This indicates that the COMB3 potential is producing a different bonding regime between Cu and graphene at the edge of the graphene sheet than it is producing in the middle of the sheet. In the middle there is only the weak van der Waals interaction as described in section 3.1, while at the graphene edges the interaction between C atoms with unsaturated bonds and the Cu surface is strong enough to make the sheet edge bend towards the Cu surface to shorten and further strengthen the Cu-C bonds. The edge type of the graphene sheet (zigzag on Cu (100), arm chair on Cu (111)) did not seem to have much influence on the results.

3.3 Room temperature wrinkle formation

In order to study what happens after cooling down, Cu (100) systems were created with graphene on them that was compressed 0.72 and 0.65 % or 1.43 and 1.36 % in the in-plane directions. In view of the similarity between Cu (100) and Cu (111) results, we only studied compressed graphene on Cu (100) surfaces. The (100) systems had surface areas a little under 13 x 13 nm^2. The graphene was initially a perfectly flat layer. Slowly cooling the system rather than creating the graphene with the complete strain in it would have been more realistic, were it not that cooling down over a 1000 K temperature range in the course of a simulation of some ns would always result in an unrealistically high cooling rate. The systems were simulated at room temperature for up to 0.5 ns. In the system with the 0.72 and 0.65 % graphene compression, the graphene did not delaminate from the Cu. Apart from the normal, small thermal vibrations, the graphene remained flat. This agrees with the continuum elastic model by N'Diaye *et al* [43] which shows that a certain minimum strain threshold must be surpassed before it becomes energetically favourable to form wrinkles rather than keeping the graphene flat and compressed. By contrast, in the system where graphene was compressed 1.43 and 1.36 %, there was bending and buckling of the graphene at various places right from the start. In under 0.1 ns the bends and buckles had consolidated into a wrinkle which (forced by the period boundary conditions of the system, most likely) ran roughly parallel to one of the axes of the system. The very short time required to form the wrinkle seems to agree with observations for graphene on Ir by N'Diaye *et al* [43], who interpreted the sudden jump in low energy electron microscopy signals as the moment when suddenly graphene on cooling Ir goes from being flat to having wrinkles. A straight, 0 K relaxed piece of the wrinkle was 2.6 nm wide and 0.5 nm high. While on the whole the wrinkle ran parallel to one of the system axes, it contained some bends. Fig. 3 shows the 1.43/1.36 % compressed system after 0.22 ns.

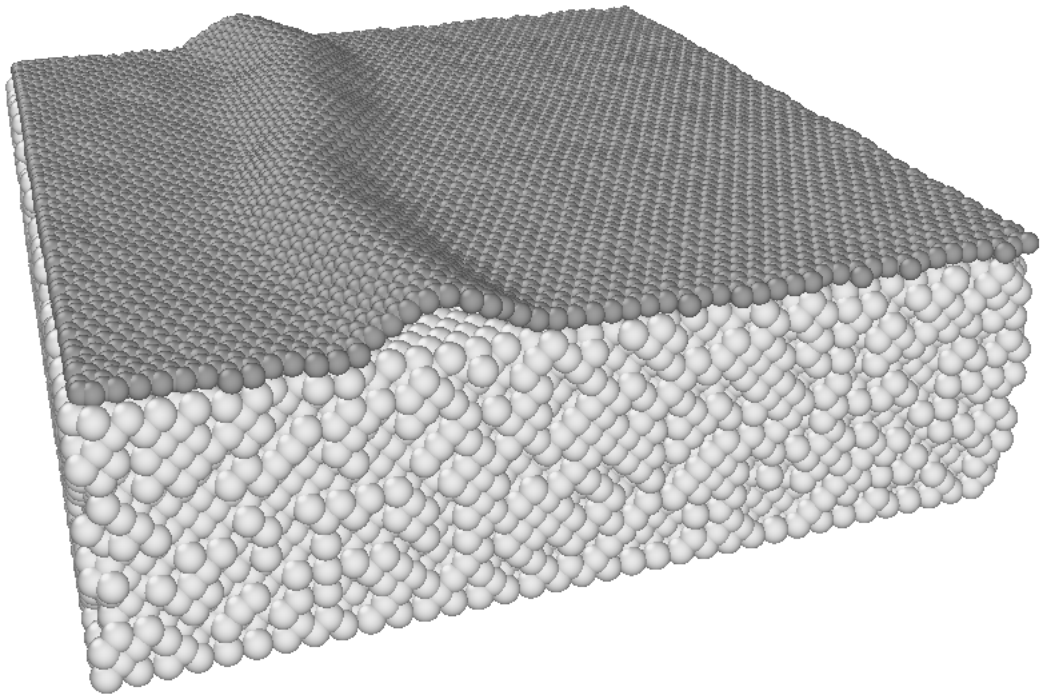

Fig. 3. Graphene with 1.43 and 1.36 % compression on Cu (100), after 0.22 ns of simulation at 300 K.

The wrinkle that is shown in fig. 3 was quite mobile. From the moment the separate bends and buckles had consolidated into the single wrinkle, it moved several nm within the tenths of ns duration of the simulation. The mobility of graphene wrinkles is in agreement with MD simulations by Guo and Guo [20] of graphene wrinkles (induced by strains that seem questionably large to us) moving over graphite and Cu surfaces, under a thermal gradient. Both in our work and that of Guo and Guo the mobility was probably higher than it would be in experiment, since it is much more likely to get a net movement over a relatively short wrinkle in a small simulation box than it is to get one for longer wrinkles in experiments. Still, the fraction of the wrinkle mobility that is present in experiments would provide a quick, easy mechanism for relieving strain in graphene by moving wrinkles to island edges where they can eliminate. The movement of our wrinkle was not uniform into one direction, but instead it moved up and down, seemingly randomly. The wrinkle also did not move uniformly as one fixed unit, but instead most of the wrinkle often moved in one direction, while (again seemingly randomly) a small part of it was standing still

or moving in the opposite direction. As a result, the shape of bending of the wrinkle changed frequently as the wrinkle moved and the height and width also showed some variation around the values of 0.5 and 2.6 nm. While the particular motions of the wrinkles that we observed seemed random, the net movement of the wrinkle and movement in opposite direction by parts of the wrinkle was not coincidental. When the velocity components on the graphene atoms were randomly re-assigned from a Boltzmann distribution, the wrinkle started making similar sorts of movements again shortly afterwards. At present we have no good explanation for these wrinkle movements. An animation of the wrinkle moving for 0.44 ns is available as supplementary content.

While the net mobility of the entire wrinkle in our simulations is likely higher than in experiments, the fluctuations within the wrinkle are probably more realistic. Since energy required to detach graphene from Cu at the front of a moving wrinkle is almost all gained back by re-attaching graphene to Cu at the back, the activation energy for movement would be very low.

The amount of elastic energy contained within the ripple could be determined from the potential energies of the individual C atoms. A Cu-graphene system with a wrinkle was cooled down to 0 K. Then the Cu substrate was removed. The potential energy of the atoms of the isolated graphene sheet, with no net charge on the C atoms, was then recalculated, see fig. 4.

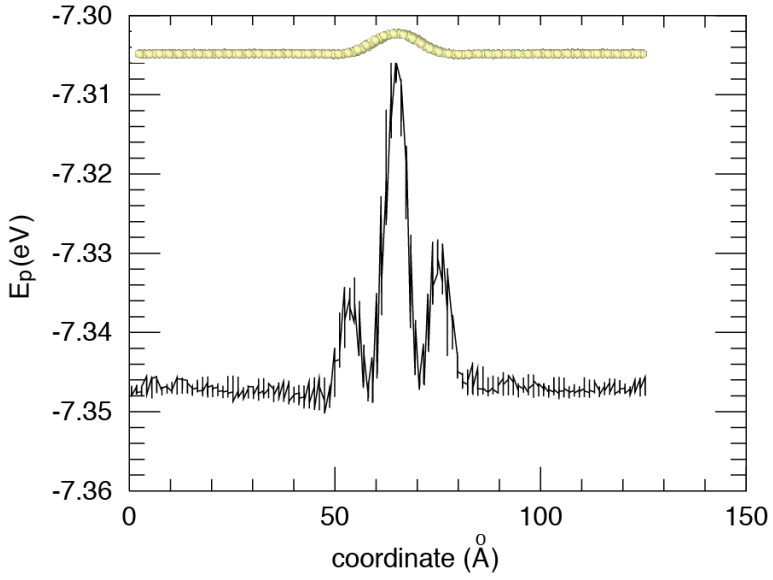

Fig. 4. Potential energy of C atoms in an isolated graphene sheet with a wrinkle in it.

The atoms in the flat graphene left and right of the wrinkle all have a more or less similar potential energy, i.e. the cohesive energy of a C atom in flat graphene. Atoms inside the wrinkle are in energetically less favourable positions. The degree to which their potential energy is less negative than that of atoms in flat graphene is the bending energy. Hence the surface area of the peaks above the energy of atoms in flat graphene is the bending energy of the wrinkle, which turned out to be 1.6 eV/nm. This is less, but of the same order of magnitude as the wrinkle bending energy found by N'Diaye *et al* [43] in their model for graphene on Ir. Note that the wrinkle has two saddle points in the radius of curvature and that around those points the graphene in the wrinkle is flat. Hence, the potential energy of C atoms around these points drops down to the value of atoms in the flat graphene left and right of the wrinkle.

In addition to the wrinkle being roughly parallel to one of the system axes, the wrinkle is likely influenced by the periodic boundary conditions in other ways as well. There is a fixed amount of extra graphene that (apart from small residual strain after wrinkle formation) is accommodated into one wrinkle. This requirement means the height and width of the wrinkle will be influenced by the size of our periodic systems. When we doubled the size of the system in fig. 4 in both dimensions, we still got a single wrinkle roughly parallel to one of the system axes but the width and height were approximately 3.6 and 0.8 nm and the bending energy was 1.9 eV/nm. Having one bigger wrinkle with 1.9 eV/nm bending energy in the larger system is energetically much more favourable than having two smaller ones with bending energies of 1.6 eV/nm each. This shows an obvious driving force for consolidating smaller wrinkles into fewer, bigger ones, as was observed in few layer graphene on Ni substrates [44].

When we again doubled both the in-plane dimensions of our system, the result no longer was a single wrinkle. Instead, two wrinkles appeared under an angle with each other. The two wrinkles intersected to form a knot that immobilised both wrinkles, see fig. 5.

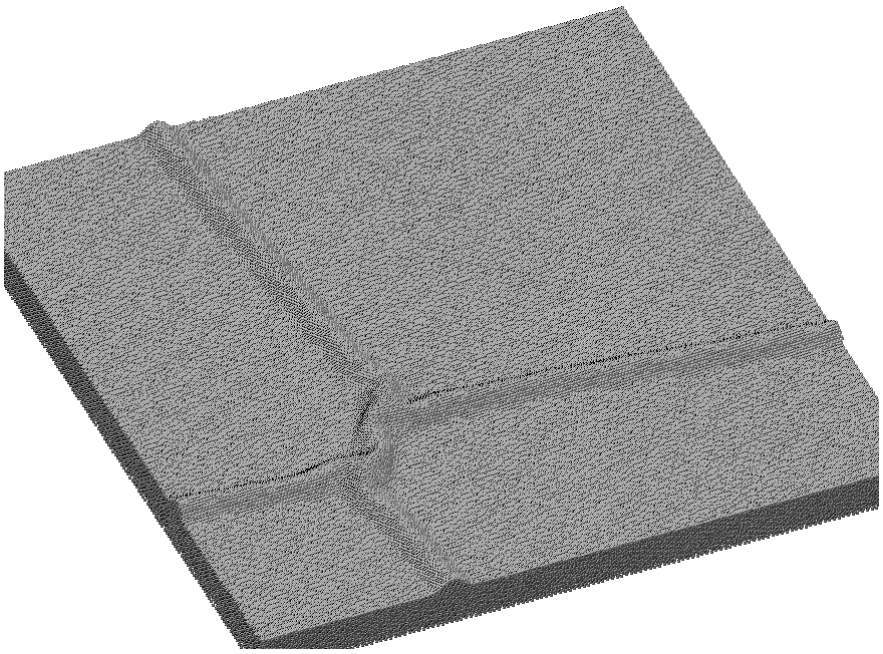

Fig. 5. Cu (100) 505 x 505 Å^2 surface with graphene sheet on it under 1.43 and 1.36% compression. The knot that connects the two wrinkles immobilises them.

Once wrinkles had grown across the full length of the surface in two dimensions, they were held in place from two sides by the knot and its periodic images. From that time onward, the wrinkles straightened out and it was no longer the case that sections of the wrinkle moved up and down nanometers, while another section might be standing still or moving in the opposite direction. The energy of the knot structure can be determined similarly to how the bending energy of a wrinkle was determined in fig. 4. First we determined the bending energy per length unit for a straight piece of the wrinkles in fig. 5. Then we determined the wrinkle length in an area containing the knot, see fig. 6.

(a)

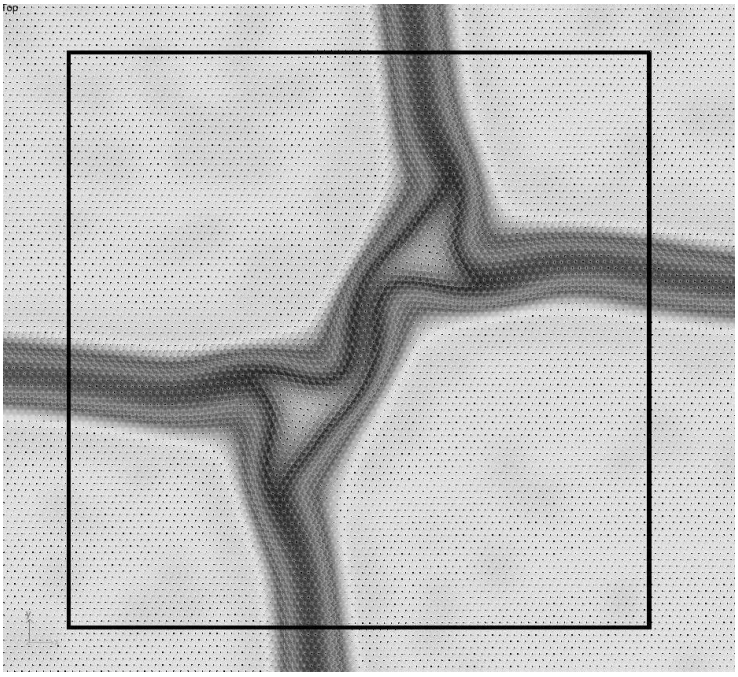

(b)

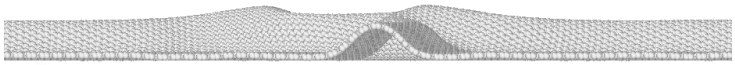

Fig. 6. (a) Area of graphene containing knot of two wrinkles, coloured by height coordinate. The bending energy of the graphene inside the area marked with a rectangle was determined, see text. (b) Side view of graphene sheet with wrinkles and knot. The maximum height of the knot above the surrounding flat graphene was higher (1.6 nm) than the height of the straight wrinkles emanating from the knot (1.0 nm).

The bending energy of a straight piece of wrinkle was 2.3 eV/nm, the total wrinkle length in the area marked in fig. 6 is ~36 nm. The bending energy of 36 nm of straight wrinkle would be 12 eV lower than the actual total bending energy we found for the graphene inside the marked area in fig. 6. Hence the knot energy for the crossing of two wrinkles under an approximately straight angle is ~12 eV. Fig. 7 shows the knot area with atoms coloured according to their potential energy.

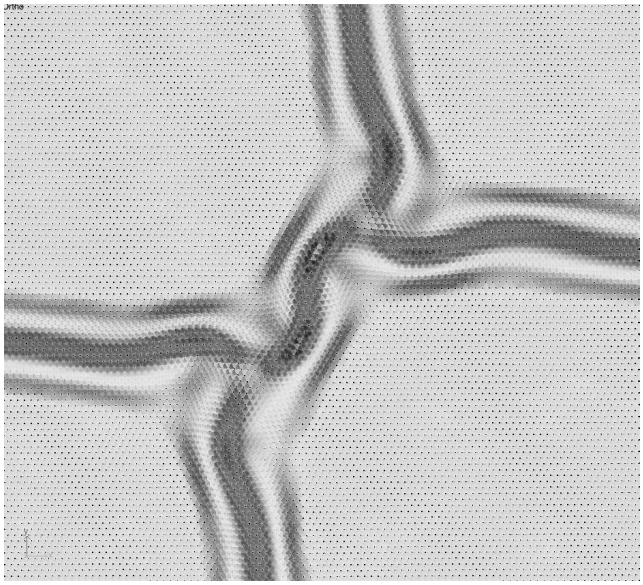

Fig. 7. Area of graphene containing knot of two wrinkles, coloured by potential energy of the atoms. The parts of the knot that are highest above the Cu surface (see fig. 6b) are not the ones with the highest potential energy, as the 'domes' do not curve very strongly. The atoms with the highest potential energy are located between the two domes, where the wrinkle forms a sharp fold.

While the high mobility of single wrinkles on flat surfaces has not been observed in experiments as far as we know (probably because catching moving wrinkles during their short mobile life times, before they eliminate at graphene island edges or form immobile knots, is quite difficult experimentally), immobilised wrinkles such as in fig. 5 have been reported for (few layer) graphene on a number of different substrates, including Ir [42, 43, 45], Pt [44], Ni [44, 46], SiC [47] and, somewhat less clearly recognisable on rougher surfaces, on Cu [48] and Rh [49]. While the similarities between immobilised wrinkles in our simulation and in experiments is encouraging, there are also some differences. First, in our simulation the knot in defect-free graphene formed at an apparently random place on the perfectly flat surface, where the wrinkle ends happened to meet up. In experiments, wrinkle nucleation may happen around defects, such as heptagon–pentagon pairs in graphene [43], and is therefore more heterogeneous. Secondly, in experiments the wrinkles often intersect under angles of 120° or other angles different from the approximately straight angle in fig. 5. This

difference probably stems from an unphysical influence of the periodic boundary conditions in our systems.
The stable persistence of immobile wrinkles would take care of some of the 1.7% thermal expansion size difference between Cu and graphene that must be accommodated during cooling. Another part of the 1.7% remains as residual strain that remains after wrinkle formation, as observed on Ir surfaces [43, 45]. Indeed, in our experiments we see graphene sticking out ~0.8% from the deposition area after cooling down, rather than 1.7%.

4 Summary

We have carried out classical molecular dynamics simulations of graphene on Cu (100) and (111) surfaces. Correctly reproducing all interactions between elements involved in CVD growth of graphene on Cu (Cu, C, H and O) is a complex task for which currently only two interaction formalisms (that share a number of characteristics) are available, ReaxFF and COMB. The COMB3 formalism gives a reasonable description of the Cu-graphene systems, though it has a number of shortcomings too.
The bonding distance between Cu and complete graphene sheets is 3.2 Å and at that distance there are no clearly distinguishable pairs of interacting Cu and C atoms. Instead, each C atom interacts with a number of Cu atoms close in distance and *vice versa* through weak van der Waals interaction. The interaction is 'averaged out' and C atoms are mostly indifferent to the fine details of how the Cu surface atoms are arranged, such as the Cu surface orientation or whether the surface is solid or molten. At graphene edges the situation is very different. There the COMB3 formalism correctly shows a much stronger interaction between C atoms with unsaturated bonds and Cu surface atoms. This causes graphene edges to bend down towards the Cu.
The tens of meV of binding per C atom between complete graphene and the Cu surface slightly stabilises the Cu surface and retards surface melting. The simulations suggest that there is a narrow temperature window where the

presence of graphene would keep the Cu surface crystalline where a bare surface would show surface melting.

Graphene layers under 1.4% compression showed the spontaneous formation of wrinkles. In simulation boxes of 13 x 13 and 25 x 25 nm^2 a single wrinkle appeared. Single wrinkles were quite mobile, moving several nm overall in tenth of ns of simulated time, in addition to smaller segments of the wrinkle moving up and down individually while other segments were standing still or moved in the opposite direction. The overall movement of wrinkles seen in our systems would be larger than in experiments, since it is easier to get a net overall movement over a short wrinkle length such as in our simulated systems. However, in experiments longer wrinkle sections would likely still have considerable mobility, since there is very little in the way of a migration barrier for graphene wrinkles to overcome. Energy required to detach graphene from the Cu surface at the front of a moving wrinkle is gained back by reattaching graphene at the back of the wrinkle. The elastic energy in the wrinkle was determined by detaching graphene and recalculating the potential energy of the C atoms. The degree to which the potential energy of atoms inside the wrinkle is less negative than that of C atoms in flat graphene, represents the bending energy. The bending energy depends on the system size (which, through the periodic boundary conditions, influences wrinkle height and width). For systems of 13 x 13 and 25 x 25 nm^2 we determined wrinkle energies of 1.6 and 1.9 eV/nm, showing that it is energetically favourable to consolidate multiple small wrinkles into a single bigger one. On a 51 x 51 nm^2 substrate, compressed graphene developed multiple wrinkles under an angle that linked up to form an immobile knot. The elastic energy of the knot structure was 12 eV. While the highly mobile single wrinkles in our simulations have not been observed in experiments as far as we know (possibly because their life times may be too small), immobilised wrinkles that are tied together under an angle have been observed in graphene on a number of different surfaces.

Acknowledgements

We thank Prashanth Srinivasan and Robbert-Jan Dikken for determining the EAM Cu melting temperature and Thomas Michely for helpful discussion and reading of the manuscript.

References

1 K. S. Novoselov, A. K. Geim, S. V. Morozov, D. Jiang, Y. Zhang, S. V. Dubonos, I. V. Grigorieva, A. A. Firsov, Science 306 (2004) 666

2 S. Choubak, M. Biron, P. L. Levesque, R. Martel, P. Desjardins, J. Phys. Chem. Lett. 4 (2013) 1100

3 S. Choubak, P. L. Levesque, E. Gaufres, M. Biron, P. Desjardins, R. Martel, J. Phys. Chem. C 118 (2014) 21532

4 I. Vlassiouk, M. Regmi, P. Fulvio, S. Dai, P. Datskos, G. Eres, S. Smirnov, ACS Nano 5 (2011) 6069

5 J. M. Wofford, S. Nie, K. F. McCarty, N. C. Bartelt, O. D. Dubon, Nano Lett. 10 (2010) 4890–4896

6 D. Geng, B. Wu, Y. Guo, L. Huang, Y. Xue, J. Chen, G. Yu, L. Jiang, W. Hu, Y. Liu, Proc. Natl. Acad. Sci. U.S.A. 109 (2012) 7992

7 S. Nie, W. Wu, S. Xing, Q. Yu, J. Bao, S. Pei, K. F. McCarty, New J. Phys. 14 (2012) 093028

8 V. E. Calado, S.-E. Zhu, S. Goswami, Q. Xu, K. Watanabe, T. Taniguchi, G. C. A. M. Janssen, L. M. K. Vandersypen, Appl. Phys. Lett. 104 (2014) 023103

9 T. Liang, B. Devine, S. R. Phillpot, S. B. Sinnott, J. Phys. Chem. A 116 (2012) 7976

10 T. Liang, T. R. Shan, Y. T. Cheng, B. D. Devine, M. Noordhoek, Y. Li, Z. Lu, S. R. Phillpot, S. B. Sinnott, Mat. Sci. Eng. R 74 (2013) 255

11 M. S. Daw, M. I. Baskes, Phys. Rev. Lett. 50 (1983) 1285

12 M. S. Daw, M. I. Baskes, Phys. Rev. B 29 (1984) 6443

13 D. W. Brenner, O. A. Shenderova, J. A. Harrison,S. J. Stuart, B. Ni, S. B. Sinnott, J. Phys.: Condens. Matter 14 (2002) 783

14 S. J. Stuart, A. B. Tutein, J. A. Harrison, J. Chem. Phys. 112 (2000) 6472

15 S. W. Chang, A. K. Nair, Markus. J. Buehler, J. Phys.: Condens. Matter 24 (2012) 245301
16 M. Reguzzoni, A. Fasolino, E. Molinari, M. C. Righi, Phys. Rev. B 86 (2012) 245434
17 S. Zhao, J. Xue, Y. Wang, S. Yan, Nanotechnology 23 (2012) 285703
18 S. K. Chien, Y. T. Yang, C. K. Chen, Nanoscale 3 (2011) 4307
19 Z. Xu, M. J. Buehler, J. Phys.: Condens. Matter 24 (2012) 475305
20 Y. Guo, W. Guo, Nanoscale 5 (2013) 318
21 T. Liang, Y. K. Shin, Y. T. Cheng, D. E. Yilmaz, K. G. Vishnu, O. Verners, C. Zou, S. R. Phillpot, S. B. Sinnott, A. C. T. van Duin, Annu. Rev. Mater. Res. 43 (2013) 12.1–12.21
22 D. Wei, Y. Song, F. Wanga, J. Chem. Phys. 134 (2011) 184704
23 B. Devine, T. R. Shan, Y. T. Cheng, A. J. H. McGaughey, M. Lee, S. R. Phillpot, S. B. Sinnott, Phys. Rev. B 84 (2011) 125308
24 S. Plimpton, J. Comput. Phys. 117 (1995) 1
25 F. C. Nix, D. MacNair, Phys. Rev. 60 (1941) 596
26 H. Jiang, B. Liu, Y. Huang, K. C. Hwang, J. Eng. Mater. 126 (2004) 265
27 D. Yoon, Y. W. Son, H. Cheong, Nano. Lett. 11 (2011) 3227
28 M. Pozzo, D. Alfè, P. Lacovig, P. Hofmann, S. Lizzit, A. Baraldi, Phys. Rev. Lett. 106 (2011) 135501
29 A. Stukowski, Modelling Simul. Mater. Sci. Eng. 18 (2010) 015012 http://ovito.org/
30 W. R. Tyson, W. R. Miller, Surf. Sci. 62 (1977) 267
31 C. K. Gan, D. J. Srolovitz, Phys. Rev. B 81 (2010) 125445
32 G. P. Dai, M. H. Wu, D. K. Taylor, K. Vinodgopal, Mater. Res. Lett. 1 (2013) 67
33 J. Cho, L. Gao, J. Tian, H. Cao, W. Wu, Q. Yu, E. N. Yitamben, B, Fisher, J. R. Guest, Y. P. Chen, N. P. Guisinger, ACS Nano 5 (2011) 3607
34 J. Zheng, Y. Wang, L. Wang, R. Quhe, Z. Ni, W. N. Mei, Z. Gao, D. Yu, J. Shi, J. Lu, Sci. Rep. 3 (2013) 2081
35 M. Vanin, J. J. Mortensen, A. K. Kelkkanen, J. M. Garcia-Lastra, K. S. Thygesen, K. W. Jacobsen, Phys. Rev. B 81 (2010) 081408(R)
36 P. A. Khomyakov, G. Giovannetti, P. C. Rusu, G. Brocks, J. van den Brink,

P. J. Kelly, Phys. Rev. B 79 (2009) 195425

37 X. Mi, V. Meunier, N. Koratkar, Y. Shi, Phys. Rev. B 85 (2012) 155436

38 S. Nie, J. M. Wofford, N. C. Bartelt, O. D. Dubon, K. F. McCarty, Phys. Rev. B 84 (2011) 155425

39 X. Zhang, Z. Xu, L. Hui, J. Xin, F. Ding, J. Phys. Chem. Lett. 3 (2012) 2822

40 A. T. Murdock, A. Koos, T. B. Britton, L. Houben, T. Batten, T. Zhang, A. J. Wilkinson, R. E. Dunin-Borkowski, C. E. Lekka, N. Grobert, ACS Nano 7 (2013) 1351

41 T. Olsen, J. Yan, J. J. Mortensen, K. S. Thygesen, Phys. Rev. Lett. 107 (2011) 156401

42 E. Loginova, S. Nie, K. Thürmer, N. C. Bartelt, K. F. McCarty, Phys. Rev. B 80 (2009) 085430

43 A. T. N'Diaye, R. van Gastel, A. J. Martínez-Galera, J. Coraux, H. Hattab, D. Wall, F.-J. Meyer zu Heringdorf, M. Horn-von Hoegen, J. M. Gómez-Rodríguez, B. Poelsema, C. Busse, T. Michely, New J. Phys. 11 (2009) 113056

44 S. J. Chae, F. Günes¸, K. K. Kim, E. S. Kim, G. H. Han, S. M. Kim, H.-J. Shin, S.-M. Yoon, J.-Y. Choi, M. H. Park, C. W. Yang, D. Pribat, Y. H. Lee, Adv. Mater. 21 (2009) 2328

45 H. Hattab, A. T. N'Diaye, D. Wall, C. Klein, G. Jnawali, J. Coraux, C. Busse, R. van Gastel, B. Poelsema, T. Michely, F.-J. Meyer zu Heringdorf, M. Horn-von Hoegen, Nano Lett. 12 (2012) 678

46 A.N. Obraztsov, E.A. Obraztsova, A.V. Tyurnina, A.A. Zolotukhin, Carbon 45 (2007) 2017

47 G. F. Sun, J. F. Jia, Q. K. Xue, L. Li, Nanotechnology 20 (2009) 355701

48 Y. Zhang, T. Gao, Y. Gao, S. Xie, Q. Ji, K. Yan, H. Peng, Z. Liu, ACS Nano 5 (2011) 4014

49 M. Liu, Y. Zhang, Y. Chen, Y. Gao, T. Gao, D. Ma, Q. Ji, Y. Zhang, C. Li, Z. Liu, ACS Nano 6 (2012) 10581